Original Article

Institution of MECHANICAL ENGINEERS
Journal of MECHANICAL ENGINEERING SCIENCE

Proc IMechE Part C:
J Mechanical Engineering Science
2015, Vol. 229(6) 1002–1014

DOI: 10.1177/0954406214542840
pic.sagepub.com
SAGE

A non-linear vehicle dynamics model for accurate representation of suspension kinematics

Prashanth KR Vaddi and Cheruvu S Kumar

Abstract

A non-linear full vehicle model for simulation of vehicle ride and handling performance is proposed. The model effectively estimates the suspension spring compressions, thus improving the accuracy of normal force calculations. This is achieved by developing models for suspension kinematics, which are then integrated with the commonly used 14 degrees of freedom vehicle dynamics models. This integrated model effectively estimates parameters like camber angles, toe angles and jacking forces, which are capable of significantly affecting the handling performance of the vehicle. The improvements in the accuracy of spring compressions help in simulating the effects of non-linear suspension elements, and the accuracy of handling simulation is enhanced by the improvements in normal force estimates. The model developed in Simulink is validated by comparing the results to that from ADAMS car.

Keywords

Vehicle dynamics, 14 DOF vehicle model, suspension kinematics, Jacking forces, normal force estimation

Date received: 27 September 2013; accepted: 18 June 2014

Introduction

There are several vehicle models for the study of handling and ride characteristics of vehicles. Three DOF yaw models are the most simple and provide a reasonable understanding of handling performance.[1,2] They have been widely used in real-time control system development. Two DOF quarter car models and seven DOF models are used for studying the ride behaviour of the vehicle.[3,4] Fourteen DOF full vehicle models with non-linear tire models have been used to improve the handling analysis by considering weight transfers and suspension spring and damper characteristics.[5] These 14 DOF models were further improved to include the effects of suspension kinematics by using the concept of roll centres.[6,7] The 14 DOF models are widely used for vehicle roll-over studies[8] and handling studies.[9] Such 14 DOF models accurately represent the suspension kinematics at low-lateral accelerations but become less accurate with increasing acceleration, due to the shortcomings of kinematic roll-centre concept.[8,10] Though these models have been widely used to simulate vehicle handling, they neglect many important factors that affect handling. Parameters like normal force distribution, camber, toe angles, jacking forces, chassis attitude angles and changes in centre of gravity (CG) position play a major role in the handling of a vehicle.[11] The distribution of the load transfer between the front and rear axles during roll is dependent on front and rear-roll stiffness,[12] where the effective roll stiffness at an axle is dependent on the suspension kinematics. Suspension components like non-linear springs are widely used to improve vehicle ride and handling performance,[13] with the non-linearity being a function of spring compression. Models, which do not consider the suspension kinematics, cannot model non-linear springs as they are poor in estimating the actual spring compressions. Though models, which use the kinematic roll centre, provide a better estimation of spring compressions, they deviate from actual values with increasing lateral accelerations. These vehicle models based on solving ODEs, although less accurate than multi-body dynamics models of ADAMS car, are more suitable for real-time simulations and hence are widely used.[14]

In this work, an improved model of the suspension kinematics is presented, which increases the accuracy of full vehicle model in representing the ride and handling characteristics. A 14 DOF model is modified

Department of Mechanical Engineering, IIT Kharagpur, West Bengal, India

Corresponding author:
Prashanth KR Vaddi, Mechanical Engineering Department, IIT Kharagpur, Kharagpur, West Bengal 721302, India.
Email: itachi369@gmail.com

to represent the effects of suspension kinematics. Models to represent suspension kinematics into a full vehicle dynamics model have been developed. This model has a better accuracy in estimation of chassis attitude, wheel orientation angles, suspension compressions, normal forces, etc. The first section of this paper is on suspension modelling, in which the kinematics is simplified for easy integration with full vehicle model. In the next section, the dynamic variations in suspension geometry are modelled. The next few sections discuss the integration of the suspension characteristics into the full vehicle model, and the necessary modelling equations are developed. The ''Results'' section compares various handling characteristics obtained from the model to that from a full vehicle multi-body dynamics model in ADAMS car.

Suspension modelling

A double wishbone suspension (Figure 1) is used to demonstrate the modelling technique. In a double wishbone suspension, the chassis can be considered to be connected to a single wheel by five links and a shock absorber with parallel spring and damper. The forces from the wheels to the chassis are transferred through the five links and the shock absorber. Changes in the attitude of the chassis are due to the compressions of the four shock absorbers, and so for the modelling of chassis, the forces that are transferred through the shock absorber should be known. F_{upf} and F_{upr} represent the forces in the forward and rearward rod of the upper wishbone. F_{lwf} and F_{lwr} similarly represent the forces in the lower wishbone, F_{st} is the force in tie-rod and F_{spr} is the force through spring and damper system; and N, F_x and F_y are the contact patch forces. A rigorous way of determining the suspension forces based on the contact patch forces is carried out by solving for six forces using six equations from three moment balance and three force balance equations.[10] To simplify the analysis, it is considered that the shock absorber is mounted along the direction of normal force, i.e. vehicle Z direction, mountings in any other orientation can be transformed to an equivalent vertical system.

Since the forces in the shock absorbers are of more interest than the forces in individual suspension links, one can simplify the computation by projecting the forces in the links onto two perpendicular planes. The forces in the suspension links can be better visualised by projecting them onto the front and side view planes in the vehicle reference frame (Figure 2(a) and (b)). Let the projected forces be F_{upyz}, F_{lwyz} and F_{styz} in the front plane/YZ plane similarly forces in side view/XZ plane be F_{upxz}, F_{lwxz} and F_{stxz}. The projections of the two wishbones in the front view and side view intersect at points O_{fv} and O_{sv}. These points are called instantaneous centres of suspension in front

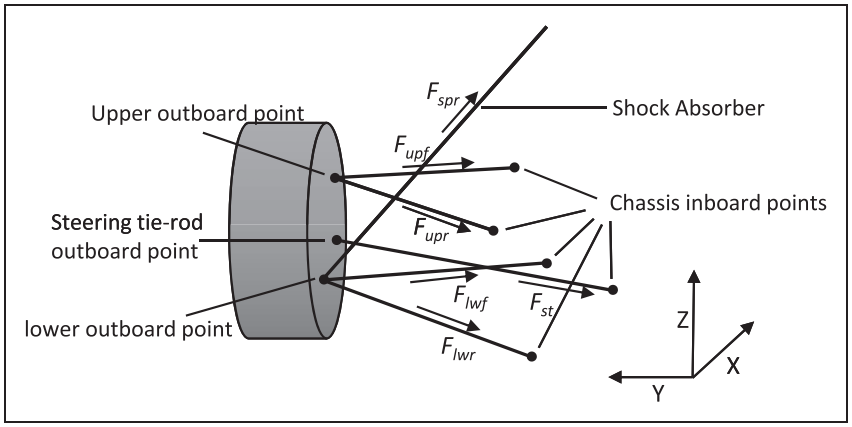

Figure 1. Double wishbone suspension.

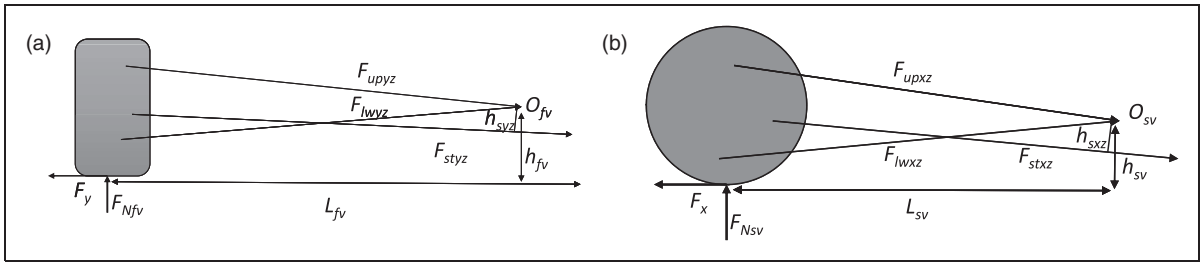

Figure 2. (a) Projection of suspension forces onto the front view plane (YZ plane) in vehicle reference frame. (b) Projection of suspension forces onto the side view plane (XZ plane) in vehicle reference frame.

and side view, and the line joining them is called instantaneous axis.[11]

In addition to the forces represented in Figure 1, inertial forces of the unsprung mass are also present. The magnitude of the unsprung mass inertial forces is too less compared to the contact patch forces. Although their affect can be considered by including some additional terms, they have been neglected in the suspension modelling to reduce the complexity.

Splitting the contact patch normal force into three components F_{Nsv}, F_{Nfv} and F_s, where F_s is the force through the shock absorber, and the other two forces represent the component of normal force through suspension links. Transferring all the forces in the suspension links, and the lateral force F_y to point O_{fv} (Figure 2(a)), the net moment is given as

$$F_{styz} \times h_{syz} - F_y \times h_{fv}$$

Similarly, in side view (Figure 2(b)), an unbalance moment is given as

$$F_{stxz} \times h_{sxz} - F_x \times h_{sv}$$

For equilibrium, these moments have to be balanced by moments due to components of normal force, F_{Nsv} and F_{Nfv}. Balancing the moment in side-view and front-view planes, respectively, the forces F_{Nsv}, F_{Nfv} are given by equation (1)

$$\begin{aligned} F_{Nfv} &= \frac{F_{styz} \times h_{syz} - F_y \times h_{fv}}{L_{fv}} \\ F_{Nsv} &= \frac{F_{stxz} \times h_{sxz} - F_x \times h_{sv}}{L_{sv}} \end{aligned} \tag{1}$$

The force in steering tie-rod can be calculated from the wheel aligning moment balance equation. The analysis gets simplified to determining the location of the two points O_{fv} and O_{sv} when the case of zero bump steer is considered. Bump steer is the case when the wheels change their steer angle without driver intervention, and this happens whenever the suspension system is in action. Zero bump steer is achieved by having the steering tie rod project to the instantaneous axis.[15] At the zero bump steer condition, h_{syz} and h_{sxz} become zero, and the forces F_{Nsv} and F_{Nfv} are given by equation (2)

$$\begin{aligned} F_{Nfv} &= \frac{-F_y \times h_{fv}}{L_{fv}} \\ F_{Nsv} &= \frac{-F_x \times h_{sv}}{L_{sv}} \end{aligned} \tag{2}$$

These components of vertical force through the suspension links are called jacking forces and are widely discussed in literature.[8,11,16] Components of vertical forces from the suspension links at the four corners of the vehicle act on the chassis, with the jacking forces depending on the contact patch forces and locations of instantaneous centres in ground reference frame. When contact patch lateral forces F_y are equal at both the wheels on an axle and with static instantaneous centres, the results obtained are same as that obtained by the traditional kinematic roll-centre[11,17] approach. The kinematic roll-centre approach fails when the vehicle is asymmetric. At high accelerations, the load transfer is high, and the normal forces at the four wheels are significantly different in turn leading to different lateral forces, thus making the kinematic roll-centre approach inaccurate.[10]

Dynamic variation in suspension geometry

The suspension geometry keeps constantly changing, so are the coordinates of the points O_{fv} and O_{sv}, which determine its effect on the suspension forces; thus, it is necessary to determine the variations in geometry to model its effects precisely. When the analysis is done in chassis reference frame, the five inboard points are fixed, and it is required to solve for the coordinates of the three suspension outboard points based on the information on steering rack travel and suspension spring compression. Solving for the points numerically is not effective as it will slow down the model simulation, and so a closed-form solution has to be developed. A closed-form solution is developed assuming certain approximations. The spring compression is considered as the change in the Z coordinate of the outboard point of lower wishbone (Figure 1), the X and Y coordinates were computed geometrically using the new Z coordinate of outboard point and the lengths of wishbone rods. The Z coordinate change in upper wishbone outboard point is estimated using the kinematic instantaneous axis, the X and Y coordinates are then determined geometrically. The coordinates of tie-rod outboard point are found similarly by approximating the change in its Z coordinate and from the steering rack travel computed through the steering wheel input.

In addition to the shock absorber force, wheel-orientation changes can also be computed using the developed model. Camber and toe angle also affect the forces generated at the contact patches.[11,18] By dynamically estimating the coordinates of three outboard points, the wheel-orientation angles can be determined. Camber, toe angles and the coordinates of instantaneous centres, which are determined in the chassis reference frame, are transformed to ground reference frame before being used in full vehicle model. The transformation matrix is computed using the chassis ride along with roll and pitch angles, which are determined from the ride-dynamics model. The camber and toe angles thus calculated can be used in non-linear tire models for accurate estimation of contact patch forces.

Integration with full vehicle model

Figure 3 shows a quarter-car model where the force F_s represents the vertical force carried by the suspension links. In vehicle models, which neglect the suspension kinematics, the force F_s is always zero; but in practical cases, its value is significantly large and depends on the suspension kinematics and contact patch forces. In a traditional quarter-car model, the force between unsprung mass and chassis is as given in equation (3)

$$F_z = C(\dot{x}_s - \dot{x}_{us}) + K(x_s - x_{us}) \tag{3}$$

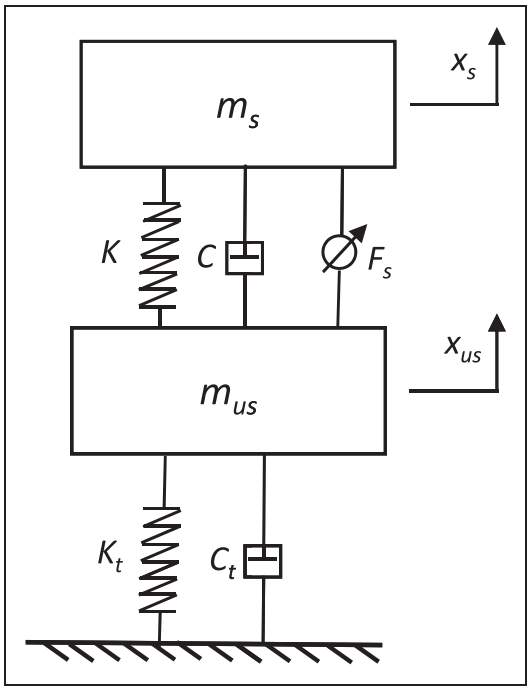

Figure 3. Quarter car model.

Due to the presence of suspension links from equation (2), the actual force is given by equation (4)

$$F_z = C(\dot{x}_s - \dot{x}_{us}) + K(x_s - x_{us}) - F_y \frac{h_{fy}}{l_{fv}} - F_x \frac{h_{sv}}{l_{sv}} \tag{4}$$

Balancing of forces and moments on the chassis about the CG gives equation (5)

$$\begin{aligned} F_{1z} + F_{2z} + F_{3z} + F_{4z} &= -mg - m\ddot{x} \\ aF_{1z} + aF_{2z} - bF_{3z} - bF_{4z} &= -ma_x h - I_{yy}\ddot{\varnothing} \\ cF_{1z} - dF_{2z} + cF_{3z} - dF_{4z} &= -ma_y h - I_{xx}\ddot{\theta} \end{aligned} \tag{5}$$

Expanding the vertical forces F_{iz} as in equation (4) and substituting them into equation (5) and writing them in matrix form give equation (6)

$$\begin{pmatrix} C_1 & C_2 & C_3 & C_4 \\ aC_1 & aC_2 & -bC_3 & -bC_4 \\ cC_1 & -dC_2 & cC_3 & -dC_4 \end{pmatrix} \begin{pmatrix} x_{1sp} \\ x_{2sp} \\ x_{3sp} \\ x_{4sp} \end{pmatrix} + \begin{pmatrix} K_1 & K_2 & K_3 & K_4 \\ aK_1 & aK_2 & -bK_3 & -bK_4 \\ cK_1 & -dK_2 & cK_3 & -dK_4 \end{pmatrix} \begin{pmatrix} x_{1sp} \\ x_{2sp} \\ x_{3sp} \\ x_{4sp} \end{pmatrix} + \begin{pmatrix} 1 & 1 & 1 & 1 \\ a & a & -b & -b \\ c & -d & c & -d \end{pmatrix} \begin{pmatrix} -\frac{h_{1fv}}{l_{1fv}} F_{1y} \\ \frac{h_{2fv}}{l_{2fv}} F_{2y} \\ -\frac{h_{3fv}}{l_{3fv}} F_{3y} \\ \frac{h_{4fv}}{l_{4fv}} F_{4y} \end{pmatrix} \tag{6}$$

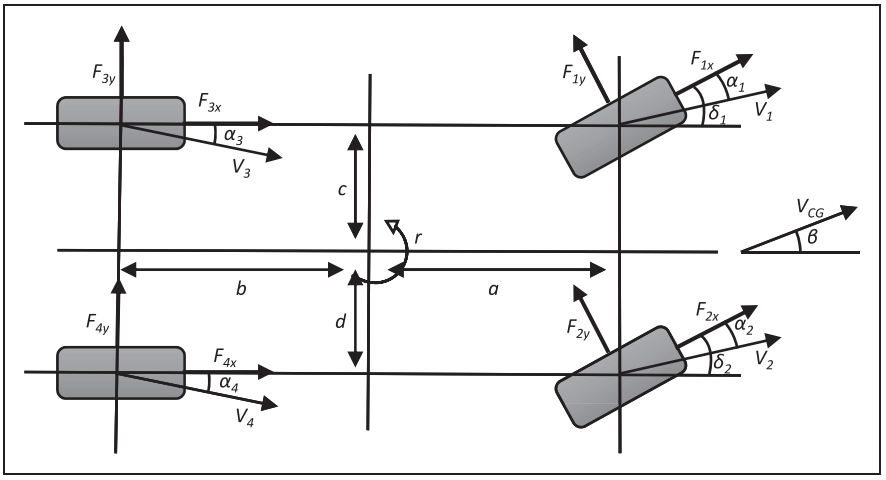

Figure 4. Vehicle in yaw plane (top plane).

$$+\begin{pmatrix}1 & 1 & 1 & 1\\ a & a & -b & -b\\ c & -d & c & -d\end{pmatrix}\begin{pmatrix}-\frac{h_{1sv}}{l_{1sv}}F_{1x}\\ -\frac{h_{2sv}}{l_{2sv}}F_{2x}\\ \frac{h_{3sv}}{l_{3sv}}F_{3x}\\ \frac{h_{4sv}}{l_{4sv}}F_{4x}\end{pmatrix}$$
$$=-\begin{pmatrix}mg\\ ma_x h\\ ma_y h\end{pmatrix}-\begin{pmatrix}m\ddot{x}\\ I_{yy}\ddot{\varnothing}\\ I_{xx}\ddot{\theta}\end{pmatrix} \quad (6)$$

The matrix containing x, θ, $\varnothing$ the ride, roll and pitch angles represent the attitude of the chassis, and it can be used to calculate x_{is} at the four corners (equation (7))

$$\begin{pmatrix}x_{1s}\\ x_{2s}\\ x_{3s}\\ x_{4s}\end{pmatrix}=\begin{pmatrix}1 & a & c\\ 1 & a & -c\\ 1 & -b & d\\ 1 & -b & -d\end{pmatrix}\begin{pmatrix}x\\ \varnothing\\ \theta\end{pmatrix} \quad (7)$$

Writing the equations for the unsprung mass in matrix form gives equation (8)

$$\begin{pmatrix}C_1 & 0 & 0 & 0\\ 0 & C_2 & 0 & 0\\ 0 & 0 & C_3 & 0\\ 0 & 0 & 0 & C_4\end{pmatrix}\begin{pmatrix}\dot{x}_{1sp}\\ \dot{x}_{2sp}\\ \dot{x}_{3sp}\\ \dot{x}_{4sp}\end{pmatrix}+\begin{pmatrix}K_1 & 0 & 0 & 0\\ 0 & K_2 & 0 & 0\\ 0 & 0 & K_3 & 0\\ 0 & 0 & 0 & K_4\end{pmatrix}$$
$$\times\begin{pmatrix}x_{1sp}\\ x_{2sp}\\ x_{3sp}\\ x_{4sp}\end{pmatrix}+\begin{pmatrix}-\frac{h_{1fv}}{l_{1fv}}F_{1y}\\ \frac{h_{2fv}}{l_{2fv}}F_{2y}\\ -\frac{h_{3fv}}{l_{3fv}}F_{3y}\\ \frac{h_{4fv}}{l_{4fv}}F_{4y}\end{pmatrix}+\begin{pmatrix}-\frac{h_{1sv}}{l_{1sv}}F_{1x}\\ -\frac{h_{2sv}}{l_{2sv}}F_{2x}\\ \frac{h_{3sv}}{l_{3sv}}F_{3x}\\ \frac{h_{4sv}}{l_{4sv}}F_{4x}\end{pmatrix}$$
$$-\begin{pmatrix}K_{1t} & 0 & 0 & 0\\ 0 & K_{2t} & 0 & 0\\ 0 & 0 & K_{3t} & 0\\ 0 & 0 & 0 & K_{4t}\end{pmatrix}\begin{pmatrix}x_{1us}\\ x_{2us}\\ x_{3us}\\ x_{4us}\end{pmatrix}$$
$$-\begin{pmatrix}C_{1t} & 0 & 0 & 0\\ 0 & C_{2t} & 0 & 0\\ 0 & 0 & C_{3t} & 0\\ 0 & 0 & 0 & C_{4t}\end{pmatrix}\begin{pmatrix}\dot{x}_{1us}\\ \dot{x}_{2us}\\ \dot{x}_{3us}\\ \dot{x}_{4us}\end{pmatrix}$$
$$=\begin{pmatrix}m_{1u} & 0 & 0 & 0\\ 0 & m_{2u} & 0 & 0\\ 0 & 0 & m_{3u} & 0\\ 0 & 0 & 0 & m_{4u}\end{pmatrix}\begin{pmatrix}\ddot{x}_{1us}\\ \ddot{x}_{2us}\\ \ddot{x}_{3us}\\ \ddot{x}_{4us}\end{pmatrix} \quad (8)$$

Many modern vehicle designs have interconnected suspension systems, and the earliest and the most used form of such a system is the anti-roll bar. The interconnections can be modelled by modifying the matrices containing K's and C's of equations (6) and (8) to represent the interconnections between suspension corners.

Equation (6) is integrated to find chassis velocities $[\dot{X}_s]$, which are used in equation (7) to find the unsprung mass velocities $[\dot{X}_{us}]$, and these velocities are used to compute the spring and damper forces. From $[\dot{X}_{us}]$, contact patch normal force can be determined (equation (9))

$$\begin{pmatrix}N_1\\ N_2\\ N_3\\ N_4\end{pmatrix}=-\begin{pmatrix}K_{1t} & 0 & 0 & 0\\ 0 & K_{2t} & 0 & 0\\ 0 & 0 & K_{3t} & 0\\ 0 & 0 & 0 & K_{4t}\end{pmatrix}\begin{pmatrix}x_{1us}\\ x_{2us}\\ x_{3us}\\ x_{4us}\end{pmatrix}$$
$$-\begin{pmatrix}C_{1t} & 0 & 0 & 0\\ 0 & C_{2t} & 0 & 0\\ 0 & 0 & C_{3t} & 0\\ 0 & 0 & 0 & C_{4t}\end{pmatrix}\begin{pmatrix}\dot{x}_{1us}\\ \dot{x}_{2us}\\ \dot{x}_{3us}\\ \dot{x}_{4us}\end{pmatrix} \quad (9)$$

Tire model

Another important part of a vehicle model is modelling the interaction between the road and the tires. An empirical model called Pacejka model is used to model the highly non-linear nature of the tire.[18] The tire model uses lateral and longitudinal slip ($\propto$ and S) along with camber angle and normal force to determine the longitudinal, lateral forces and tire moments at the contact patch. The lateral and longitudinal forces are as shown in equation (10), and the coefficients B_i, C_i, D_i, E_i and S_i are dependent on normal forces and are determined through multiple tests on tires being used. Normal forces are computed in the ride model; camber and toe angles are available from kinematic analysis; the lateral slip angles are estimated from the model of vehicle yaw motion; and longitudinal slip from tire rotational model. The forces calculated from the magic formula are steady-state values. To model the transient nature of the forces, a first-order lag, which depends on the tire rotational speed, is applied on the steady-state estimations[18]

$$\begin{aligned}F_y &= D_y \sin\left[C_y \arctan\left\{B_y \propto \right.\right.\\ &\quad \left.\left. - E_y\left(B_y \propto - \arctan\left(B_y \propto\right)\right)\right\}\right] + S_y\\ F_x &= D_x \sin\left[C_x \arctan\left\{B_x S\right.\right.\\ &\quad \left.\left. - E_x(B_x S - \arctan(B_x S))\right\}\right]\end{aligned} \quad (10)$$

Yaw model

The dynamics of the vehicle in the road plane can be represented by a yaw model with three DOF (Figure 4), and the three motions are the longitudinal and

lateral motion of the CG and rotational yaw motion of the vehicle along Z axis. Equations of motion in the lateral and longitudinal directions are given by equation (11) and equation (12), respectively, where the terms used are as defined in "Notation"

$$\begin{aligned} mV(r+\dot{\beta}) &= \left[(F_{1x}\sin(\delta_1)+F_{2x}\sin(\delta_2)+F_{1y}\cos(\delta_1)\right. \\ &\quad \left.+F_{2y}\cos(\delta_2)+\left(F_{3y}+F_{4y}\right)\right]\cos(\beta) \\ &\quad -[F_{1x}\cos(\delta_1)+F_{2x}\cos(\delta_2)-F_{1y}\sin(\delta_1) \\ &\quad -F_{2y}\sin(\delta_2)+F_{3x}+F_{4x}]\sin(\beta) \end{aligned} \tag{11}$$

$$\begin{aligned} m\dot{V} &= \left[(F_{1x}\sin(\delta_1)+F_{2x}\sin(\delta_2)+F_{1y}\cos(\delta_1)\right. \\ &\quad \left.+F_{2y}\cos(\delta_2)+\left(F_{3y}+F_{4y}\right)\right]\sin(\beta) \\ &\quad +[F_{1x}\cos(\delta_1)+F_{2x}\cos(\delta_2)-F_{1y}\sin(\delta_1) \\ &\quad -F_{2y}\sin(\delta_2)+F_{3x}+F_{4x}]\cos(\beta) \end{aligned} \tag{12}$$

Yaw acceleration is computed by writing in the equation of angular motion along vehicle Z axis. The results of equation (13) for yaw acceleration are integrated to find the yaw rate, which along with the velocity computed by integrating longitudinal acceleration in equation (12) can be used in equation (11) to find body-slip rate and also body-slip angle by integration

$$\begin{aligned} \dot{r} &= \frac{1}{I_{zz}}[a(F_{1y}\cos(\delta_1-\beta)+F_{2y}\cos(\delta_2-\beta) \\ &\quad +F_{1x}\sin(\delta_1-\beta)+F_{2x}\sin(\delta_2-\beta))-b(F_{3y}\cos(\beta) \\ &\quad +F_{4y}\cos(\beta)-F_{3x}\sin(\beta)-F_{4x}\sin(\beta)) \\ &\quad -c(F_{1x}\cos(\delta_1-\beta)+F_{3x}\cos(\beta)-F_{1y}\sin(\delta_1-\beta) \\ &\quad +F_{3y}\sin(\beta))+d(F_{2x}\cos(\delta_2-\beta)+F_{4x}\cos(\beta) \\ &\quad -F_{2y}\sin(\delta_2-\beta)+F_{4y}\sin(\beta)) \end{aligned} \tag{13}$$

The steering input angles along with the yaw rate and body slip can be used to compute individual lateral tire-slip angles. These tire-slip angles are used in the tire model. Lateral slip angles at the four wheels are as shown in equation (14)

$$\begin{aligned} \alpha_1 &= \delta_1-\beta-\frac{ra}{V}; \quad \alpha_2 = \delta_2-\beta-\frac{ra}{V} \\ \alpha_3 &= \delta_3-\beta+\frac{rb}{V}; \quad \alpha_4 = \delta_4-\beta+\frac{rb}{V} \end{aligned} \tag{14}$$

Table 1. Vehicle parameters of the ADAMS car template used for model validation.

Sprung mass m	1430 kg
Sprung mass roll inertia I_{xx}	400 kgm^2
Sprung mass yaw inertia I_{zz}	1000 kgm^2
Sprung mass pitch inertia I_{yy}	600 kgm^2
Distance of CG from front axle a	1.48 m
Distance of CG from rear axle b	1.08 m
CG height h	0.456 m
Front/rear track width c, d	0.78 m
Front suspension stiffness	121,000 N/m
Rear suspension stiffness	110,000 N/m
Front suspension damping coefficient	3000 Ns/m
Rear suspension damping coefficient	3000 Ns/m
Front unsprung mass	25 kg
Rear unsprung mass	30 kg
Front/rear tire stiffness	310,000 N/m
Nominal tire radius R	0.33 m
Rear roll centre distance below CG	0.265 m
Front roll centre distance below CG	0.295 m

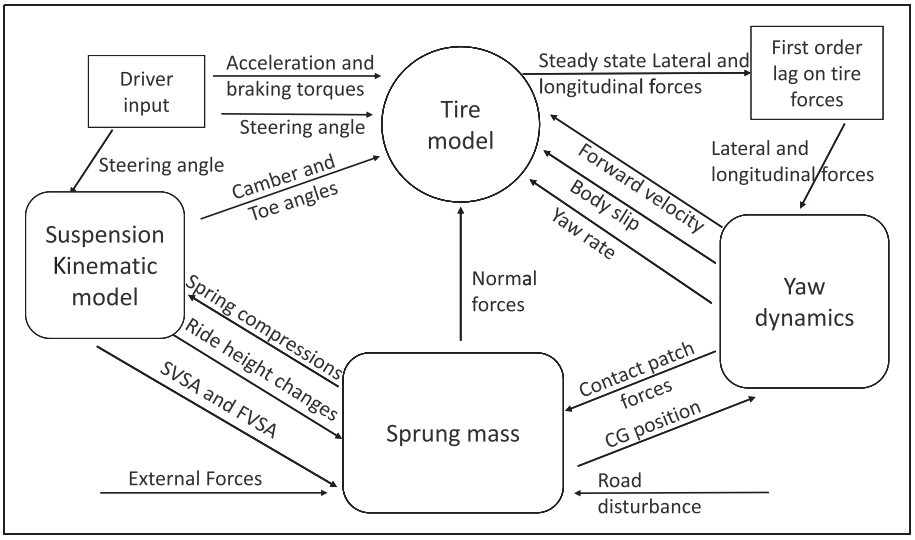

Figure 5. Model integration.

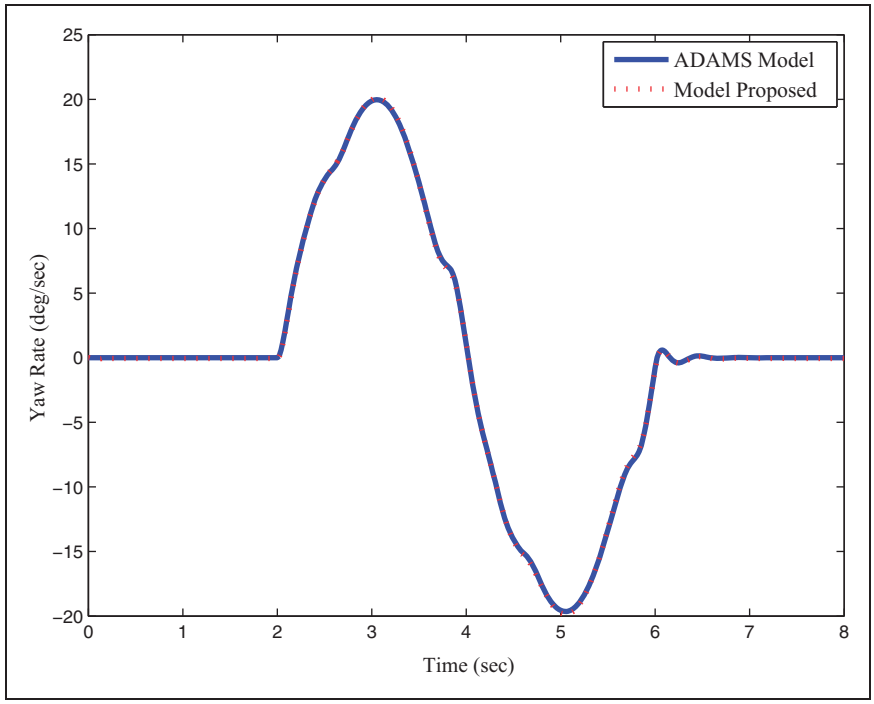

Figure 6. Yaw rate during single lane change test.

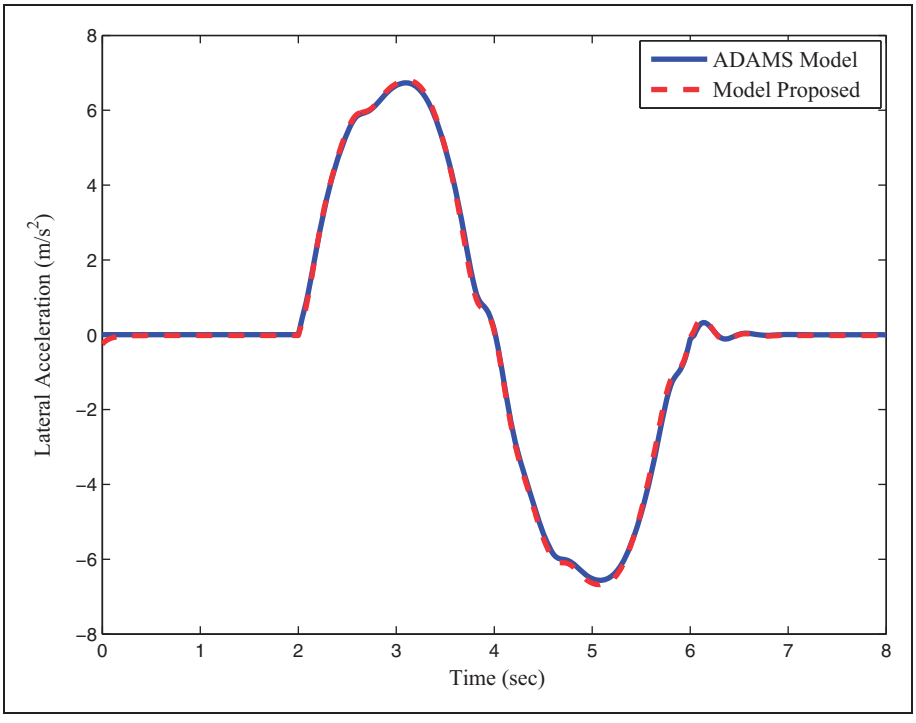

Figure 7. Lateral acceleration during single lane change test.

If ω is the angular velocity of the wheel, then the wheel longitudinal slip ratio used in the tire model is given by equation (15), and the equation of motion for calculating ω is given by equation (16). In equation (16), I_w is the polar inertia of the rotating components, T is the torque from either the engine or brakes, R is the tire nominal radius and F_x represents the longitudinal force at a wheel, which can be calculated using the tire model

$$S = \frac{\omega R - V}{V} \tag{15}$$

$$I_W \dot{\omega} = T - F_x R \tag{16}$$

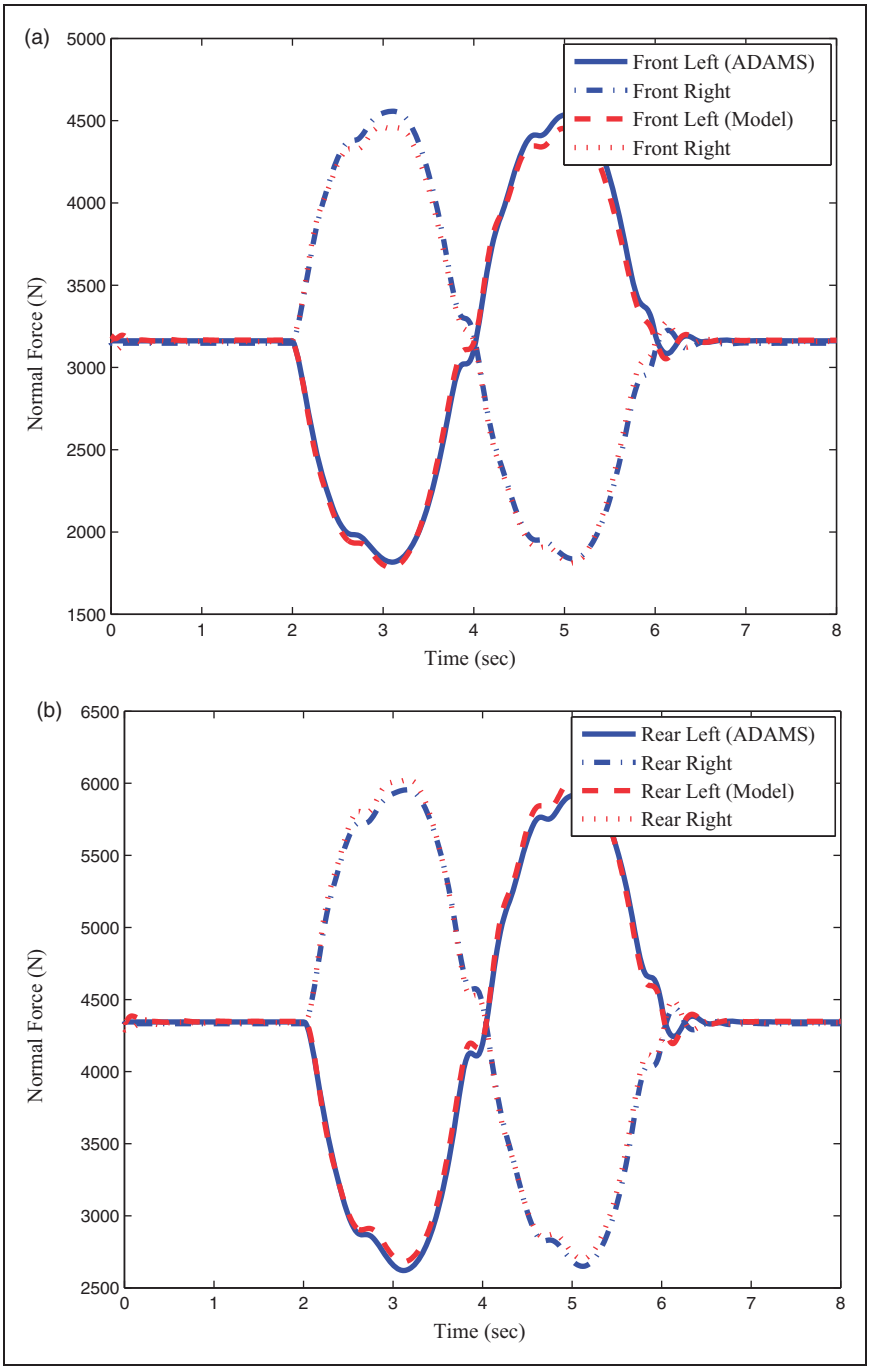

Figure 8. (a) and (b): Normal forces on the front and rear wheels in a single lane change test.

Model integration

The 14 DOF full vehicle model is developed in Simulink by building sub models of seven DOF ride dynamics model, suspension kinematics, tire model with four DOF representing the rotational freedom of the four wheels and three DOF yaw model. These sub-models interact through the flow of data. The interaction between the various sub-models and the nature of inputs and outputs of the sub-models can be seen in Figure 5. This Simulink model is used to study the effects of suspension kinematics on the handling of the vehicle.

Results

In order to test the efficiency of the model, a set of simulations were carried out, towards this a standard vehicle has been assumed, which was taken from a standard template available with ADAMS car. Some critical parameters of the model are as shown in Table 1. A single lane-change test was used to validate the model, and the results obtained are compared with ADAMS car model. Spring compression

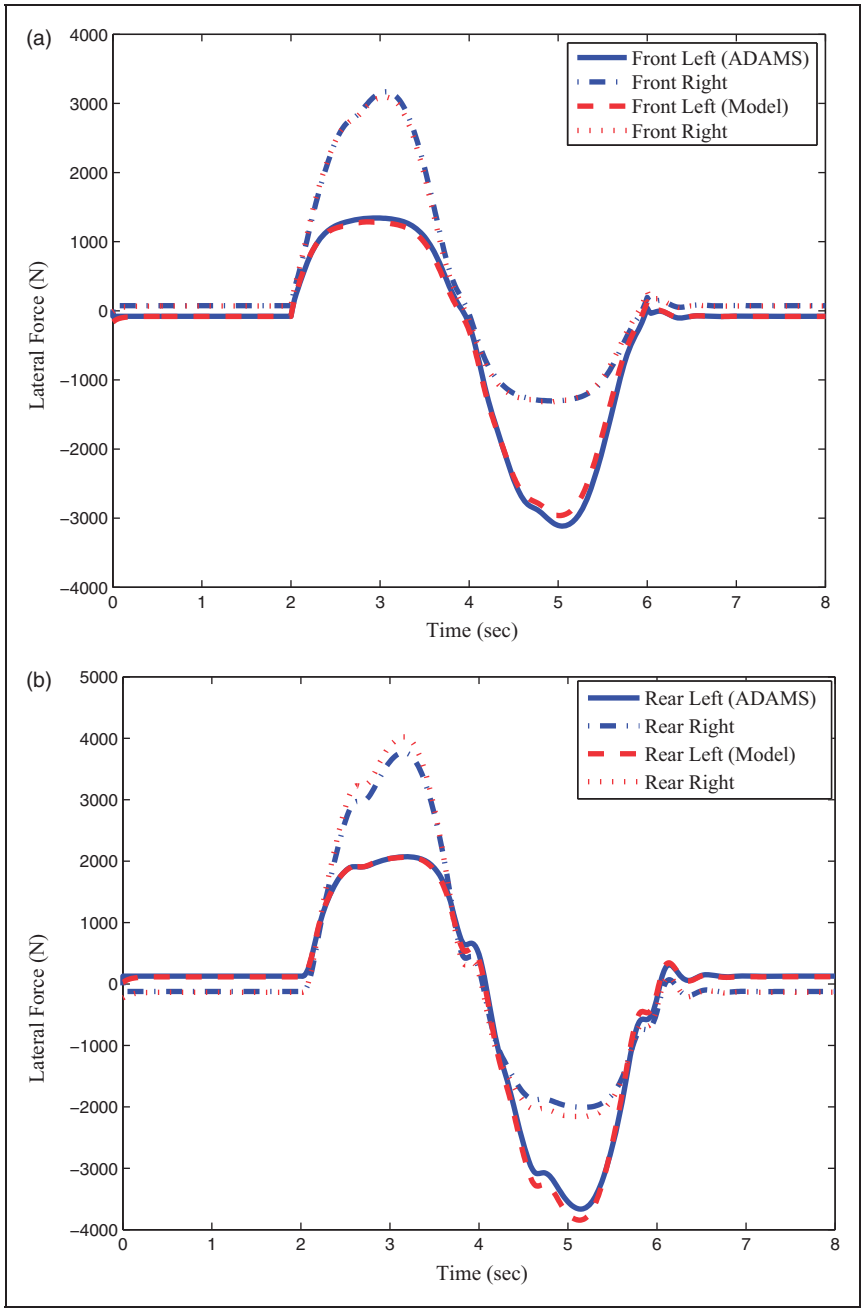

Figure 9. (a) and (b): lateral forces on the front and rear wheels in a single lane change test.

and normal force estimates are also compared to standard 14 DOF vehicle models to show the improvements. The Simulink model was setup with vehicle parameters and Pacejka tire coefficients from the template model provided with ADAMS car. For the single lane test, a steering angle input of a sine wave with maximum angle of 100° and a time period of 4 s at a vehicle speed of 72 kmph were used. Individual wheel steer angles from ADAMS car were used as input to the model developed. The comparison of yaw rate and lateral acceleration is provided in Figures 6 and 7.

Lateral and normal forces at all the four contact patches are compared as they form an important part in representing the influence of suspension kinematics. The normal force and lateral force comparisons for all the four wheels can be found in Figures 8 and 9.

The spring compressions at the four wheels are critical in the study of non-linear suspensions. They are also important for computing toe and camber angles at different wheel orientations. The accuracy in estimation of spring compressions is shown by comparing the results from the model to the results from ADAMS car, results for 14 DOF vehicle models, which do not consider suspension effects, and results from models, which use the kinematic roll centre concept, are also used for a comparative study. The results for front left, front right, rear left and rear right suspensions can be found in Figure 10.

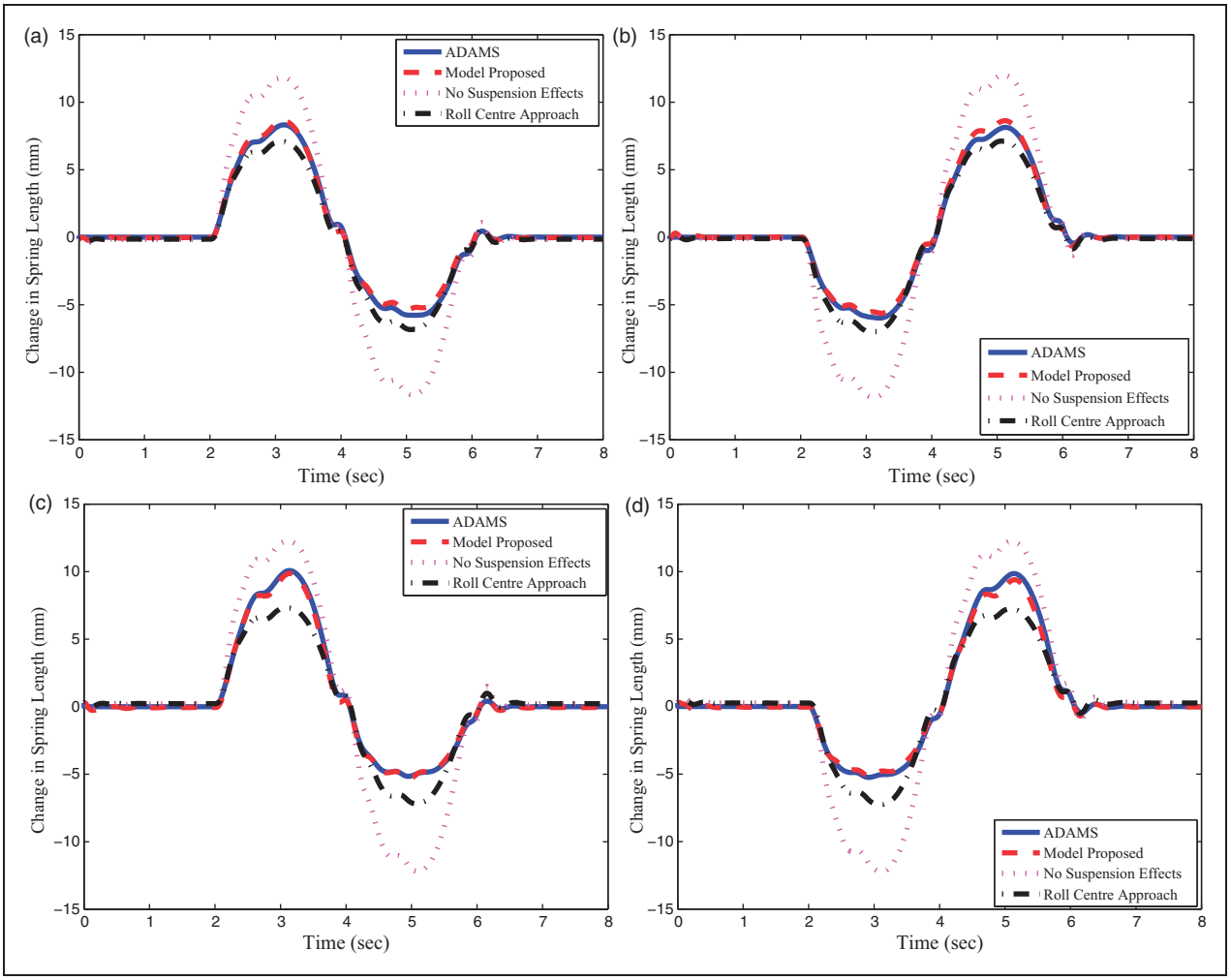

Figure 10. (a) and (b): comparison of spring lengths in front left and front right suspensions; (c) and (d): comparison of spring lengths in rear left and rear right suspensions.

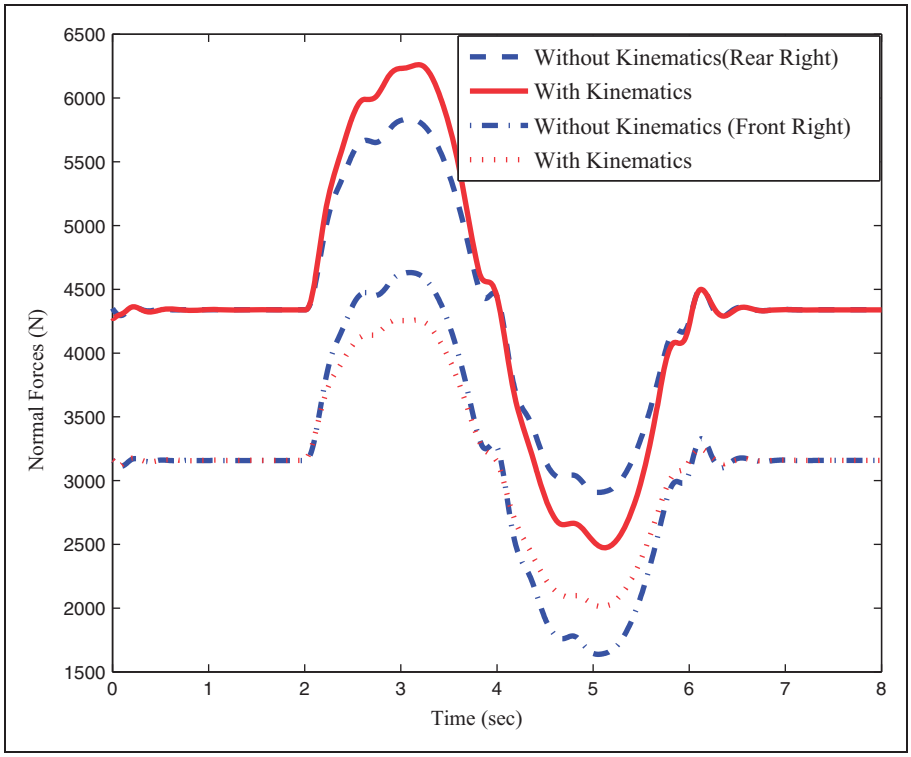

Figure 11. Normal force comparison to show the effects of suspension kinematics.

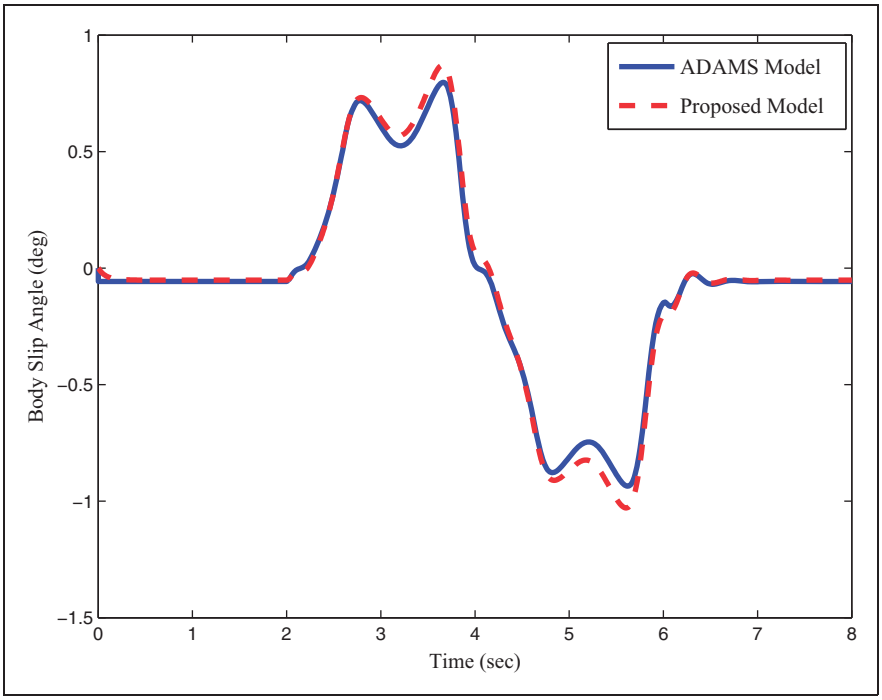

Figure 12. Comparison of body slip angle.

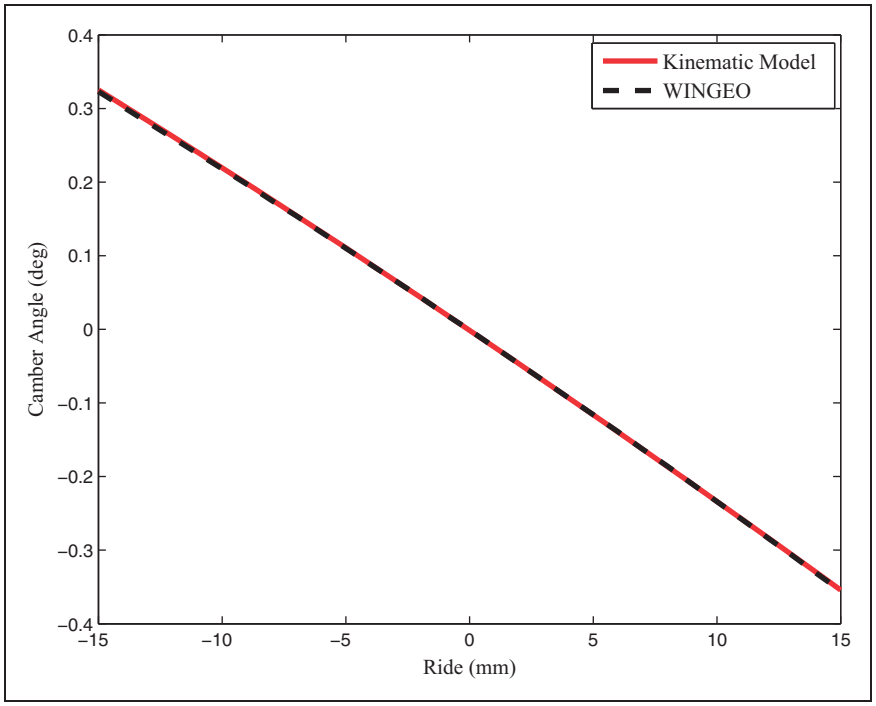

Figure 13. Comparison of camber angles.

An accurate simulation of spring compressions also results in an accurate estimation of chassis orientation parameters like ride height, roll angle and pitch angle; this also accurately estimates the change in the position of CG.

The difference between normal force estimates of model developed and a model, which does not represent the suspension kinematics, can be seen in Figure 11. The normal forces for wheels on the right side are shown in Figure 12. To clearly show the difference, the suspension kinematics has been adjusted to get a roll-centre heights of 86 and 266 mm in the front and rear suspensions.

A comparison of body-slip angle is provided in Figure 12 to show the accuracy of the model in representing the vehicle-handling behaviour.

For the validation of the kinematic model developed and to check for the accuracy of camber angle estimates, the results from the kinematic model are compared to that from suspension kinematics software WINGEO3 by Mitchell software (Figure 13).[19]

Slight differences in the model developed and the ADAMS car model might be the result of some of the approximations made and factors neglected. Due to the use of rubber bushings in the suspension system, there is significant camber compliance present in the ADAMS model. The model developed does not consider the compliance in suspension leading to errors in lateral force estimations. The assumption of Zero bump steer throughout the motion of suspension and neglecting of unsprung mass in developing the equations for kinematic influence can also affect the model accuracy. External forces like aerodynamic drag and moment have not been modelled and can influence the results.

Conclusion

A full vehicle model with better estimates of the suspension spring compressions and normal forces is developed. This can be seen from the comparisons with other 14 DOF models, which do not consider the effects of suspension kinematics. Other important estimates like that of lateral forces, yaw rate and body-slip angle are in good agreement with the ADAMS car simulations. The suspension models developed for the purpose also provide estimates of camber angles, which improve the accuracy of lateral force estimations. Thus, the model improves the accuracy of ride and handling simulations over the commonly used 14 DOF models.

Conflict of interest

None declared.

Funding

This research received no specific grant from any funding agency in the public, commercial, or not-for-profit sectors.

References

1. Hac A and Bodie MO. Improvements in vehicle handling through integrated control of chassis systems. *Int J Veh Auton Syst* 2002; 1: 83–110.
2. Anwar S. Generalized predictive control of yaw dynamics of a hybrid brake-by-wire equipped vehicle. *Mechatronics* 2005; 15: 1089–1108.
3. Yoshimura T, Kume A, Kurimoto M, et al. Construction of an active suspension system of a quarter car model using the concept of sliding mode control. *J Sound Vib* 2001; 239: 187–199.
4. Chalasani RM. Ride performance potential of active suspension systems, Part I: Simplified analysis based on a quarter-car model. In: *Proceedings of the ASME symposium on simulation of ground vehicles*, Los Angeles, 1986.
5. Kadir ZA. Verification of 14DOF full vehicle model based on steering wheel input. *Appl Mech Mater* 2012; 165: 109–113.
6. Setiawan JD, Safarudin M and Singh A. Modeling, simulation and validation of 14 DOF full vehicle model. In: *International conference on instrumentation, communication, information technology, and biomedical engineering (ICICI-BME)*, Bandung, Indonesia, 2009, pp.1–6.
7. Wang W and Song Y. A new high dimension nonlinear dynamics simulation model for four-wheel-steering vehicle. *Proc IMechE, Part C: J Mechanical Engineering Science* 2012; 227: 29–37.
8. Shim T and Ghike C. Understanding the limitations of different vehicle models for roll dynamics studies. *Veh Syst Dyn: Int J Veh Mech Mobil* 2007; 45: 191–216.
9. Bin FX, Jiang Y and Wang HG. Stability optimal control based on 15-dof vehicle model. *Adv Mater Res* 2011; 299–300: 1266–1270.
10. Mitchell WC. Force-based roll centers and an improved kinematic roll center. SAE Technical Paper 2006, 2006-01-3617.
11. Milliken WF and Milliken DL. Race car vehicle dynamics. *SAE Int* 1995; 1: 607–661.
12. Bodie MO and Hac A. Closed loop yaw control of vehicles using magneto-rheological dampers. *SAE Trans* 2000; 109: 132–139.
13. Zapletal E. Balanced suspension, SAE Technical Paper 2000-01-3572, 2000.
14. Sayers MW. Vehicle models for RTS applications. *Veh Syst Dyn: Int J Veh Mech Mobility* 1999; 32: 4–5. 421–438.
15. Lindorfer MD and Anderson BL. Zero bump steer suspension. Patent 5,000,476, USA, 19 March 1991.
16. Hac A. Rollover stability index including effects of suspension design. No. 2002-01-0965. SAE Technical Paper, 2002.
17. Dixon J. The roll-centre concept in vehicle handling dynamics. *Proc IMechE, Part D: J Automobile Engineering* 1987; 201: 69–78.
18. Bakker E, Pacejka HB and Lidner L. A new tire model with an application in vehicle dynamics studies. In: *Autotechnologies conference and exposition*, Monte Carlo, Monaco, 1989, No. P-221.
19. Mitchell WC. WinGeo3 5.01 – Suspension geometry with force-based roll centers. http://www.mitchellsoftware.com/prod01.htm (accessed 27 June 2014).

Appendix

Notation

a	distance from front axle to CG (m)
a_x, a_y	longitudinal and lateral acceleration (m/s^2)
b	distance from rear axle to CG (m)
c, d	half axle widths (m)
C_i	damping coefficient (N s/m)
C_{it}	tire damping coefficient (N s/m)
CG	centre of gravity
F_{iX}	longitudinal tire forces (N)
F_{iY}	lateral tire forces (N)

h	centre of gravity height (m)
h_{sv}, h_{fv}	height of instantaneous centre in index I 1-front left, 2-front right, 3-rear left and 4-rear right side view and front view
I_{kk}	moment of inertia about k axis (kg m^2)
I_W	inertia of wheel
K_i	Spring stiffness (N/m)
K_{it}	tire stiffness (N/m)
l_{sv}, l_{fv}	distance of instantaneous centre in side view and front view
m_{iu}	unsprung mass (kg)
M	sprung mass (kg)
r	yaw rate (rad/s)
R_i	effective radius of the wheel
S_i	wheel longitudinal slip ratio
T_i	net wheel driving torque (N m)
V	vehicle CG speed (m/s)
w	axle width (m)
x_{isp}	Spring expansion (m)
x_{is}	sprung mass position at corner i
x_{ius}	unsprung mass position at corner i
α_i	wheel lateral slip angle (rad)
β	body slip angle at CG (rad)
δ_i	steering angle input (radians)
θ	Chassis roll angle (radians)
φ	Chassis pitch angle (radians)
ω_i	angular speed of wheel (rad/s)